

Conf-950153--1

PNL-SA-24935

ONSET TIME AND STRENGTH OF OCEANIC DEEP CONVECTION  
DIAGNOSED FROM AN OCEAN LARGE-EDDY SIMULATION  
MODEL

D. W. Denbo

January 1995

Presented at the  
Fourth Conference on Polar Meteorology and  
Oceanography  
→ January 15-20, 1995  
Dallas, Texas

Prepared for  
the U.S. Department of Energy  
under Contract DE-AC06-76RLO 1830

Pacific Northwest Laboratory  
Richland, Washington 99352

DISTRIBUTION OF THIS DOCUMENT IS UNLIMITED

## **DISCLAIMER**

**Portions of this document may be illegible in electronic image products. Images are produced from the best available original document.**

# ONSET TIME AND STRENGTH OF OCEANIC DEEP CONVECTION DIAGNOSED FROM AN OCEAN LARGE-EDDY SIMULATION MODEL

Donald W. Denbo

Pacific Northwest Laboratory  
Sequim, Washington

## 1. INTRODUCTION

Deep convection has an important role in the large-scale thermohaline circulation, which in turn plays a central part in determining global climate. Manabe and Stouffer's (1993) climate simulations have shown that the thermal and dynamical structure of the oceans have pronounced changes in model climates with increased CO<sub>2</sub>. In their simulations, the addition of low-salinity surface water at high latitudes prevents the ventilation of the deep ocean, thus reducing or in some cases nearly extinguishing the thermohaline circulation. Siegenthaler and Sarmiento (1993) remarked that whereas the ocean is the largest of the rapidly exchanging global carbon reservoirs and a major sink for anthropogenic carbon, this uptake capacity becomes available only when the whole ocean is chemically equilibrated with the new atmospheric CO<sub>2</sub> concentration. The dynamics of the oceanic uptake of CO<sub>2</sub> is therefore strongly determined by the rate of downward transport of CO<sub>2</sub>-laden water from surface to depth.

The importance of deep convection in moderating the uptake of CO<sub>2</sub> by the ocean and its role in the meridional circulation, which affects climate by transporting heat from the tropics to the polar regions, motivates this research. The experiments described here were designed to study the sensitivity of the onset time and strength of deep convection to changes in the heat flux, latent heat flux, and perturbations of the surface mixed-layer temperature and salinity.

## 2. MODEL DESCRIPTION

The ocean large-eddy simulation model (OLEM) described here is non-hydrostatic, Boussinesq and three-dimensional. The primitive equation model uses a turbulent kinetic energy sub-grid model and flux corrected transport advection scheme. The momentum equations are those presented in Denbo and Skillingstad (1994):

*Corresponding author address:* Donald W. Denbo,  
Pacific Northwest Laboratory, Battelle/Marine Sciences  
Laboratory, 1529 W. Sequim Bay Road, Sequim, Wash-  
ington 98382. Internet: [dwd@mystery.pnl.gov](mailto:dwd@mystery.pnl.gov)

$$\frac{\partial u}{\partial t} = -\frac{\partial \bar{P}}{\partial x} + R_u, \quad (1)$$

$$\frac{\partial v}{\partial t} = -\frac{\partial \bar{P}}{\partial y} + R_v, \quad (2)$$

$$\frac{\partial w}{\partial t} = -\frac{\partial \bar{P}}{\partial z} + R_w - \langle R_w \rangle, \quad (3)$$

$$\frac{\partial u}{\partial x} + \frac{\partial v}{\partial y} + \frac{\partial w}{\partial z} = 0, \quad (4)$$

where the velocities  $u$ ,  $v$  and  $w$  are in the  $x$ ,  $y$  and  $z$  (zonal, meridional and upward) directions, respectively, and where

$$R_u = -u \frac{\partial u}{\partial x} - v \frac{\partial u}{\partial y} - w \frac{\partial u}{\partial z} - \mathcal{P}_x + 2\Omega_z v - 2\Omega_y w + 2 \frac{\partial}{\partial x} \left[ K_m \frac{\partial u}{\partial x} \right] + \frac{\partial}{\partial y} \left[ K_m \left( \frac{\partial u}{\partial y} + \frac{\partial v}{\partial x} \right) \right] + \frac{\partial}{\partial z} \left[ K_m \left( \frac{\partial u}{\partial z} + \frac{\partial w}{\partial x} \right) \right],$$

$$R_v = -u \frac{\partial v}{\partial x} - v \frac{\partial v}{\partial y} - w \frac{\partial v}{\partial z} - \mathcal{P}_y - 2\Omega_z u + \frac{\partial}{\partial x} \left[ K_m \left( \frac{\partial u}{\partial y} + \frac{\partial v}{\partial x} \right) \right] + 2 \frac{\partial}{\partial y} \left[ K_m \frac{\partial v}{\partial y} \right] + \frac{\partial}{\partial z} \left[ K_m \left( \frac{\partial v}{\partial z} + \frac{\partial w}{\partial y} \right) \right],$$

and

$$R_w = -u \frac{\partial w}{\partial x} - v \frac{\partial w}{\partial y} - w \frac{\partial w}{\partial z} - g \frac{\rho'}{\rho_0} + 2\Omega_y u + \frac{\partial}{\partial x} \left[ K_m \left( \frac{\partial u}{\partial z} + \frac{\partial w}{\partial x} \right) \right] + \frac{\partial}{\partial y} \left[ K_m \left( \frac{\partial v}{\partial z} + \frac{\partial w}{\partial y} \right) \right] + 2 \frac{\partial}{\partial z} \left[ K_m \frac{\partial w}{\partial z} \right].$$

A modified pressure is defined as

$$\bar{P} = \frac{P}{\rho_0} + \frac{2}{3} e''$$

where

$$e'' = 1/2 \left( u''^2 + v''^2 + w''^2 \right).$$

The double primed variables denote sub-grid quantities. The angle brackets denote horizontal means,  $\Omega_z$  and  $\Omega_y$  are the vertical and horizontal components of the Coriolis parameter, respectively, and  $\mathcal{P}_x$  and  $\mathcal{P}_y$  are the zonal and meridional background pressure gradients, respectively.

**MASTER**

The diagnostic equation for pressure is formed by taking the divergence of the momentum equations (1) thru (3) and then substituting equation (4) to yield:

$$\frac{1}{\rho^0} \nabla^2 P = \frac{\partial}{\partial x} R_u + \frac{\partial}{\partial x} R_v + \frac{\partial}{\partial z} (R_w - \langle R_w \rangle).$$

The evolution of scalars is governed by

$$\frac{\partial \phi}{\partial t} = -u \frac{\partial \phi}{\partial x} - v \frac{\partial \phi}{\partial y} - w \frac{\partial \phi}{\partial z} + \frac{\partial}{\partial x} \left( K_h \frac{\partial \phi}{\partial x} \right) + \frac{\partial}{\partial y} \left( K_h \frac{\partial \phi}{\partial y} \right) + \frac{\partial}{\partial z} \left( K_h \frac{\partial \phi}{\partial z} \right),$$

where  $\phi$  can be  $\Theta$ ,  $S$ , or a tracer.

### Sub-grid Model.

The sub-grid scale turbulence parameterization follows the method described by Deardorff (1980), where an eddy viscosity scheme is used for fluxes and the eddy coefficient is set proportional to the square root of the sub-grid turbulent kinetic energy (TKE). The sub-grid TKE is calculated using a prognostic equation.

The eddy coefficients are defined as

$$K_m = C_{km} \lambda e^{-z/2} \text{ and} \\ K_h = \left( C_{hl} + C_{hs} \frac{\lambda}{\Delta s} \right) K_m$$

where  $\Delta s = (\Delta x \cdot \Delta y \cdot \Delta z)^{1/3}$  and

$$\lambda = \begin{cases} \Delta s, & \text{unstable} \\ C_l e^{-z/2} \left( \frac{g}{\rho^0} \frac{\partial \rho}{\partial z} \right)^{-1/2}, & \text{stable} \end{cases}$$

The dissipation rate,  $\varepsilon$ , is prescribed by

$$\varepsilon = \frac{C}{\lambda} e^{-3z/2} \text{ and } C = C_{\varepsilon l} + C_{\varepsilon s} \frac{\lambda}{\Delta s}.$$

The empirical constants (Deardorff 1973, 1980) are defined as  $C_{\varepsilon l} = 0.19$ ,  $C_{\varepsilon s} = 0.51$ ,  $C_l = 0.76$ ,  $C_{km} = 0.1$ ,  $C_{hl} = 1$ , and  $C_{hs} = 2$ .

In the grid points next to the solid boundaries,  $C$  is increased by a factor of 3.9 to compensate for boundary effects (Deardorff 1980).

### Numerics and Boundary Conditions

OLEM uses a three-dimensional staggered grid with pressure and scalars in the center of a cube and the velocity components on the faces. The coordinate system origin is in the lower, left-front corner of the domain. Grid spacing in the model is uniform with  $\Delta x = \Delta y = \Delta z$ . This is not a severe limitation, given the scale of problems for which OLEM is best suited.

The boundary conditions used with OLEM were chosen to be consistent with the assumption that the

model domain, horizontal scale of a few kilometers, is being placed in a region that is horizontally homogeneous at scales many times larger than the model domain. The horizontal boundary conditions were therefore chosen to be cyclic, where flow out a horizontal boundary enters the opposite boundary. We make the rigid lid approximation and use a flat bottom,

$$w = 0, \text{ at } z = 0, L_z.$$

The surface boundary conditions,  $z = L_z$ , for the surface fluxes use a formulation where the fluxes directly force the surface grid cell. The surface boundary conditions for horizontal velocity components,  $\Theta$ , and  $S$ , are

$$u^{n+1} = u^n + \frac{2\Delta t}{\Delta z} \cdot \frac{\tau_x}{\rho},$$

$$v^{n+1} = v^n + \frac{2\Delta t}{\Delta z} \cdot \frac{\tau_y}{\rho},$$

$$\Theta^{n+1} = \Theta^n + \frac{\Delta t}{\Delta z} \cdot \frac{H_f}{c_p \rho},$$

and

$$S^{n+1} = S^n \cdot \left( \frac{\rho}{\rho + \frac{\Delta t L_f}{\Delta z L_v}} \right)$$

where  $\tau_x$ ,  $\tau_y$ ,  $H_f$ , and  $L_f$  are the zonal wind stress, meridional wind stress, total heat flux, and latent heat flux, respectively. The superscripts on the model variables denote the current time step number, where  $\Delta t$  is the time step increment. The values of specific heat,  $c_p$ , and latent heat of vaporization,  $L_v$ , are chosen for seawater at 10°C, 35 PSU, and atmospheric pressure. The bottom boundary conditions,  $z = 0$ , are no-slip for the horizontal velocities and no-flux for  $\Theta$  and  $S$ .

The control of the non-physical  $2\Delta x$  motions is accomplished by applying a Shapiro filter to all three velocity components. In this study, a sixth-order Shapiro filter, with the highest order term of  $\nabla^{12}$ , was applied in all three directions every third time step.

The accurate advection of  $\Theta$  and  $S$  is very important in OLEM. Small errors in advecting these two components of density can result in significant errors in the resultant density field and velocity perturbations that are of the same magnitude as the motions of interest. Therefore, the advection of  $\Theta$ ,  $S$ ,  $e^w$ , and tracers is accomplished using a flux-corrected transport scheme based on the work of Collela (1990) using the flux limiting step from van Leer (1977). This scheme has the property that strong fronts of the advected quality, after a small amount of numerical diffusion, reach an equilibrium

shape that is then transported without significant additional numerical diffusion.

### 3. EXPERIMENTS

The relationship among heat flux, latent heat flux, and perturbations of the surface mixed-layer temperature ( $\Delta\Theta_{surf}$ ) and salinity ( $\Delta S_{surf}$ ), and the onset time and strength of deep penetrative convection were determined by conducting 26 experiments (Table 1). A small

Table 1: Summary of runs.

Ident	$H_f$ ( $W m^{-2}$ )	$L_f$ ( $W m^{-2}$ )	$\Delta\Theta_{surf}$ ( $^{\circ}C$ )	$\Delta S_{surf}$ (PSU)
base-1	-300	0	0	0
hf-1	-150	0	0	0
hf-2	-450	0	0	0
hf-3	-600	0	0	0
hf-4	-900	0	0	0
hf-5	-1200	0	0	0
lf-1	-300	-50	0	0
lf-2	-300	-100	0	0
lf-3	-300	-150	0	0
lf-4	-300	-200	0	0
dt-1	-300	0	-0.05	0
dt-2	-300	0	-0.10	0
dt-3	-300	0	-0.15	0
dt-4	-300	0	-0.20	0
dt-5	-300	0	-0.25	0
dt-6	-300	0	0.10	0
dt-7	-300	0	0.20	0
dt-8	-300	0	0.30	0
ds-1	-300	0	0	0.005
ds-2	-300	0	0	0.010
ds-3	-300	0	0	0.015
ds-4	-300	0	0	0.020
ds-5	-300	0	0	-0.015
ds-6	-300	0	0	-0.010
ds-7	-300	0	0	-0.005
ds-8	-300	0	0	-0.020

domain of 2000 m by 2000 m by 2000 m depth with a grid spacing of 50 m was used in the experiments in order to economically generate this large number of runs. The results' dependence on the grid spacing was checked using a 2000 m by 2000 m by 2000 m depth

with a grid spacing of 25 m domain, which yielded quantitatively similar results. The initial T-S profiles are based on a profile taken in the Greenland Sea (Figure 1).

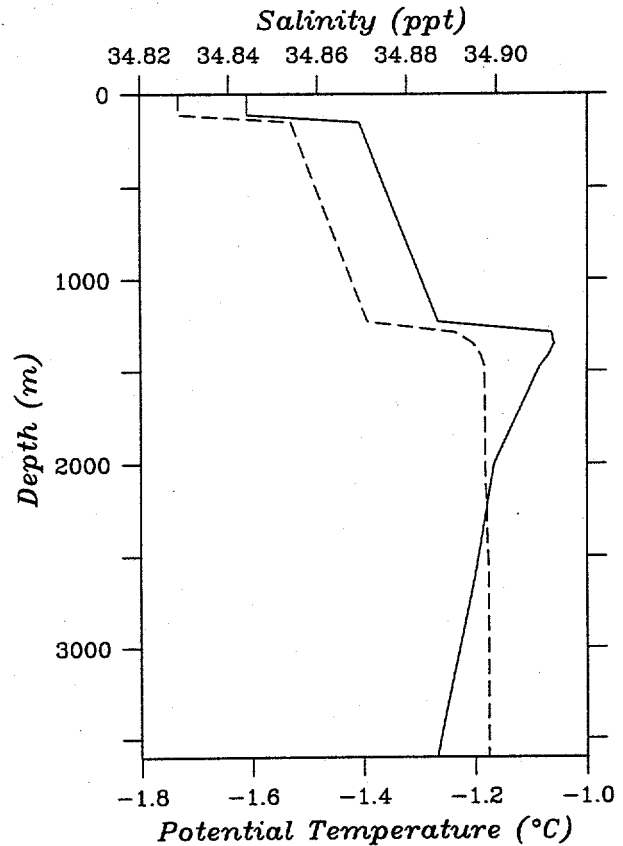


Figure 1: Initial potential temperature (solid line) and salinity (dashed line) profile, based on a profile taken at 2° W, 74° 45'N during February, 1988, in the central Greenland Sea (Rudels et al. 1989).

The time of maximum potential temperature variance in the upper 800 m is used as a proxy for the onset time of penetrative convection (Figure 2). This proxy was chosen because large perturbations in the position of the mixed-layer base, which gives rise to large potential temperature variances, occur at the onset of penetrative convection. The magnitude of this variance is used as a proxy for the strength of the penetrative convection.

If the onset time of the penetrative convection is determined only by the buoyancy change in the surface mixed layer, the onset time will be proportional to  $H_f^{-1}$  (Figure 3a),  $\Delta\Theta_{surf}$  (Figure 4a), and  $\Delta S_{surf}$  (Figure 4c). These relationships, over the parameter range in the experiments, fit the model results exceptionally well, with  $r^2=0.9996$ ,  $r^2=0.9987$ , and  $r^2=0.9970$  for the heat flux,  $\Delta\Theta_{surf}$ , and  $\Delta S_{surf}$  experiments, respectively. If the

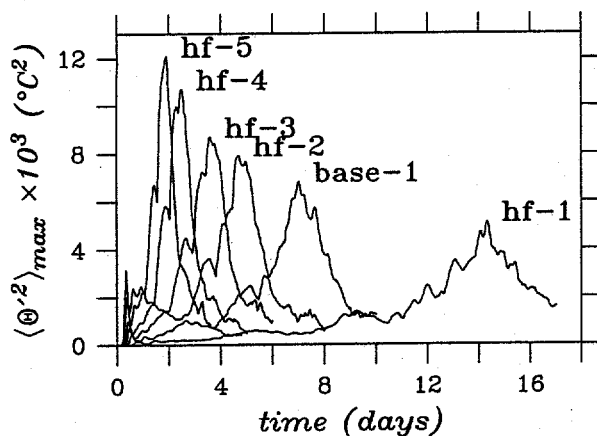


Figure 2: Maximum potential temperature variance in the top 800 m as a function of time for the five heat flux experiments and the base case.

maximum temperature variance in the upper 800 m is primarily caused by the deformation of the mixed-layer base, we might expect the temperature variance to be proportional to the vertical velocity variance, which is proportional to  $H_f^{2/3}$  (Figure 3b). The model results' fit to this relationship is extremely high ( $r^2=0.9968$ ).

Evaporation of water (negative latent heat flux) increases the surface salinity, thus reducing the static stability. The faster loss of static stability decreases the onset time of penetrative convection (Figure 3c). However, the increased salinity also reduces the strength of the thermobaric instability, and with it, the maximum temperature variance (Figure 3d).

The strength of convection decreases with increasing  $\Delta\Theta_{surf}$  (Figure 4b). Since the onset of convection is delayed with increasing  $\Delta\Theta_{surf}$  the mixed layer depth at the time of convection is correspondingly greater. The mixed layer therefore incorporates a greater amount of relatively high salinity water from below the mixed layer, reducing the strength of the thermobaric instabil-

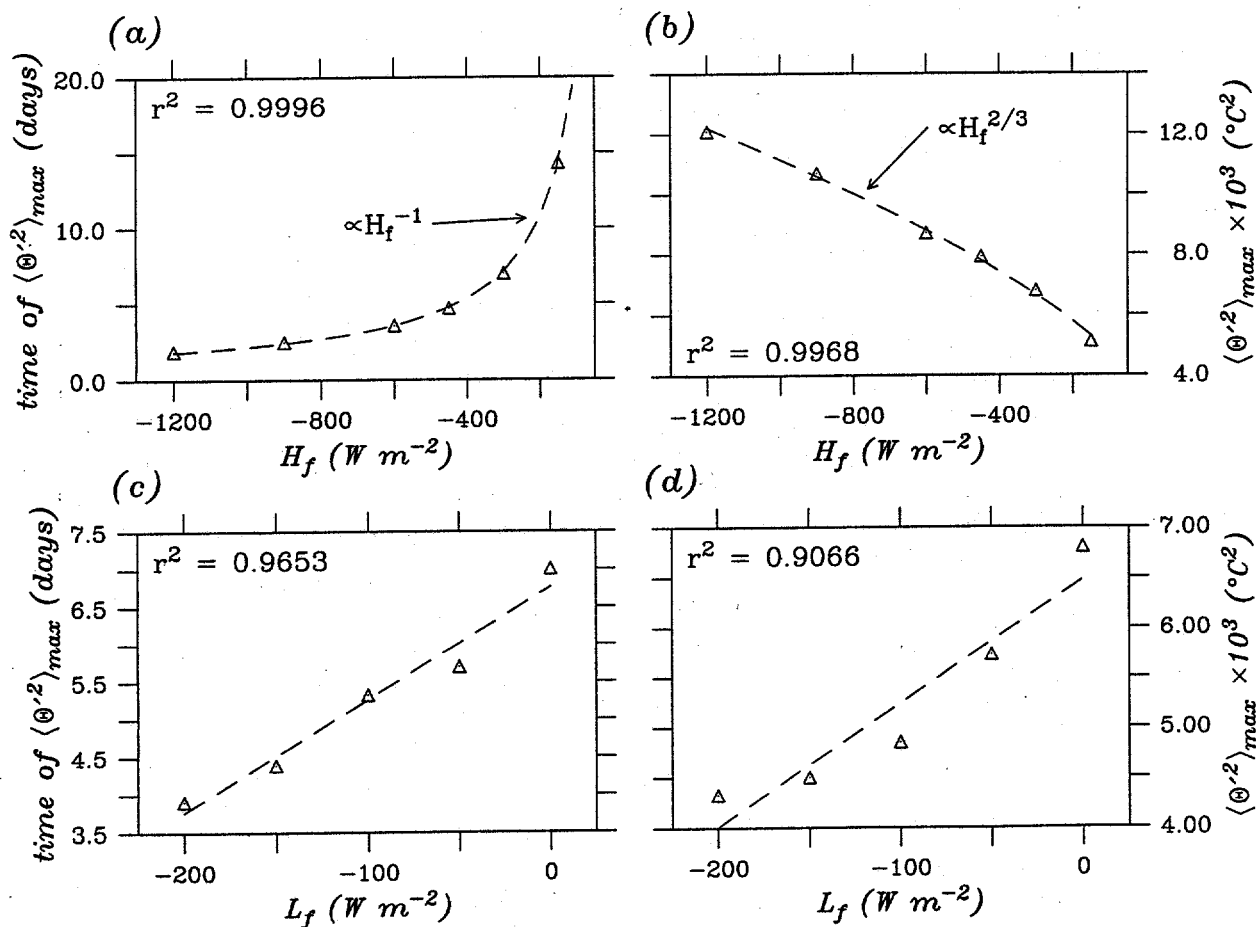


Figure 3: Time of maximum potential temperature variance in the top 800 m for the heat flux (a) and latent heat flux (b) experiments, and maximum potential temperature variance for the heat flux (c) and latent heat flux (d) experiments.

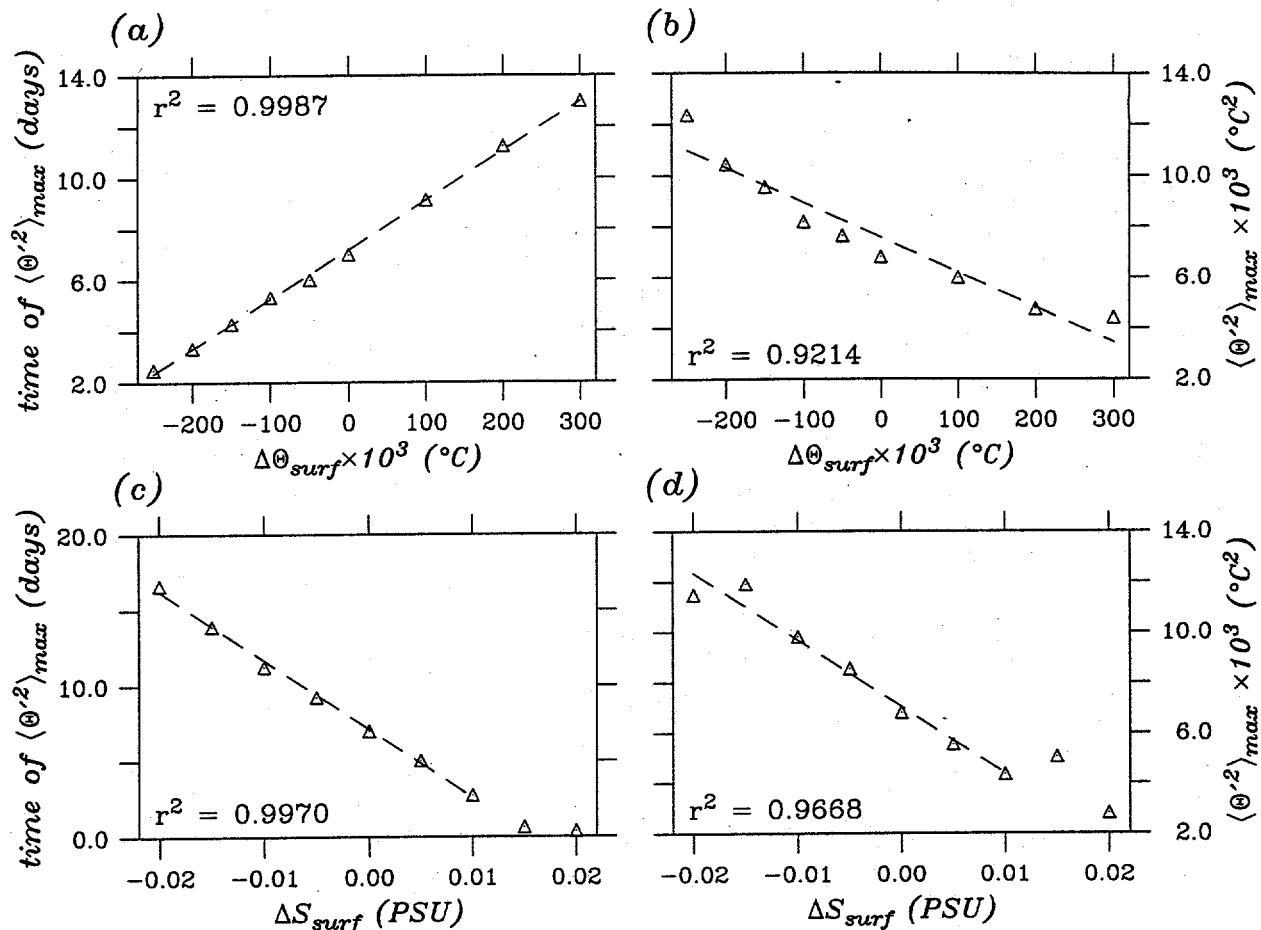


Figure 4: Time of maximum potential temperature variance in the top 800 m for the surface mixed-layer temperature (a) and salinity (b) perturbation experiments, and maximum potential temperature variance for the surface mixed-layer temperature (c) and salinity (d) perturbation experiments.

ity with increasing  $\Delta\Theta_{surf}$  and therefore the maximum temperature variance.

The strength of convection also decreases with increasing  $\Delta S_{surf}$  (Figure 4d). Increasing the surface salinity decreases the static stability and thermobaric instability. Again, the decreased thermobaric instability leads to a decrease in the maximum temperature variance.

#### 4. CONCLUSIONS

The sensitivity study results demonstrate that the onset time of deep convection is controlled by the amount of heat extracted from the ocean and is not strongly related to the rate at which heat is removed or the initial mixed-layer temperature. This result implies that high frequency forcing of OGCMs may not be necessary to produce the correct timing of deep convection.

However, the onset and strength of convection is sensitive to the strength of the thermobaric instability and those processes that can change it: namely, the mag-

nitude of the latent heat flux, mixed-layer deepening, and the T-S profile.

The empirical relationships developed from the sensitivity study results help improve our understanding of deep convections' response to changes in forcing and environmental conditions and provides a basis for improving deep convection parameterizations used in climate models.

#### 5. ACKNOWLEDGMENTS

The author wishes to thank Michael R. Riches, acting director of the Environmental Sciences Division of the Office of Health and Environmental Research, for his continual support of this work. This study was carried out under the auspices of the CO<sub>2</sub> Oceans Program at the Battelle/Marine Sciences Laboratory. The Battelle/Marine Sciences Laboratory is part of the Pacific Northwest Laboratory, which is operated for the U.S. Department of Energy by Battelle Memorial Institute under Contract DE-AC06-76RLO 1830.

## 6. REFERENCES

- Colella, P., 1990: Multidimensional upwind methods for hyperbolic conservation laws, *J. Comput. Phys.*, **87**, 171-200.
- Deardorff, J. W., 1973: The use of subgrid transport equations in a three-dimensional model of atmospheric turbulence, *J. Fluids Eng.*, **95**, 429-438.
- Deardorff, J. W., 1980: Stratocumulus-capped mixed layers derived from a three-dimensional model, *Bound-Layer Meteor.*, **18**, 495-527.
- Denbo, D. W., and E. D. Skillingstad, 1994: An oceanic large eddy simulation model with application to deep convection in the Greenland Sea, *submitted to J. Geophys. Res.*
- Manabe, S., and R. J. Stouffer, 1993: Century-scale effects of increased atmospheric CO<sub>2</sub> on the ocean-atmosphere system, *Nature*, **364**, 215-218.
- Rudels, B., D. Quadfasel, H. Friedrich, and M.-N. Housais, 1989: Greenland Sea convection in the winter of 1987-1988, *J. Geophys. Res.*, **94**(C3), 3223-3227.
- Siegenthaler, U., and J. L. Sarmiento, 1993: Atmospheric carbon dioxide and the ocean, *Nature*, **365**, 119-125.
- van Leer, B., 1977: Towards the ultimate conservative difference scheme: IV: A new approach to numerical convection, *J. Comput. Phys.*, **23**, 276-299.

## DISCLAIMER

This report was prepared as an account of work sponsored by an agency of the United States Government. Neither the United States Government nor any agency thereof, nor any of their employees, makes any warranty, express or implied, or assumes any legal liability or responsibility for the accuracy, completeness, or usefulness of any information, apparatus, product, or process disclosed, or represents that its use would not infringe privately owned rights. Reference herein to any specific commercial product, process, or service by trade name, trademark, manufacturer, or otherwise does not necessarily constitute or imply its endorsement, recommendation, or favoring by the United States Government or any agency thereof. The views and opinions of authors expressed herein do not necessarily state or reflect those of the United States Government or any agency thereof.